Life history traits influence the dynamics of genetic diversity in a refugium population undergoing expansion and contraction

Ravi Vishwakarma, Gabriele Maria Sgarlata, David Soriano-Panos, Rita Rasteiro, Tiago Maie, Tiago Paixao, Rémi Tournebize, Lounès Chikhi

Life history traits influence the dynamics of genetic diversity in a refugium population undergoing expansion and contraction

Ravi Vishwakarma [1,*], Gabriele Maria Sgarlata [1,*], David Soriano-Paños [1,*], Rita Rasteiro [1,2], Tiago Maié [1,3], Tiago Paixão [1], Rémi Tournebize [4,] Lounès Chikhi [1,4,5 1]

[1]Instituto Gulbenkian de Ciência, Oeiras, Portugal.
[2]MRC Integrative Epidemiology Unit, University of Bristol, Bristol, United Kingdom.
[3]Institute for Computational Genomics, RWTH Aachen University, Germany.
[4]Laboratoire Évolution & Diversité Biologique, CNRS, IRD, UPS, Université de Toulouse Midi-Pyrénées, Toulouse, France.
[5]Centre de Recherche sur la Biodiversité et l'Environnement, CNRS, IRD, UPS, Université de Toulouse Midi-Pyrénées, Toulouse, France.
[*]shared first author

March 28, 2024

Corresponding authors:
Ravi Vishwakarma: rvishwakarma@igc.gulbenkian.pt,
Lounès Chikhi: lounes.chikhi@univ-tlse3.fr / chikhi@igc.gulbenkian.pt
David Soriano-Paños: sorianopanos@gmail.com

Keywords: spatial processes, population structure, refugium, generation time, dispersal, demographic history, lag

Abstract

Species ranges are dynamic, experiencing expansions, contractions or shifts as a response to habitat changes induced by extrinsic factors such as climate change and, more recently, human activities. While the scientific literature has explored the genetic effects of spatial processes, published studies rarely incorporate life-history traits to study the effect of such changes on species living in the same environments. There is thus a gap in our understanding regarding the variation in genetic diversity patterns among species with distinct life-history traits such as growth rates and generation times, experiencing the same habitat change scenarios. In this study, we first used spatial simulations to investigate the temporal dynamics of genetic diversity within refugium populations experiencing a range expansion followed by a stationary and a contraction period. We explored different scenarios, varying both the speed of contraction and the life-history traits of the simulated species. In addition we used a simpler panmictic model for which we derived analytical results. Altogether, we identified three temporal dynamics of genetic diversity in the refugium population during the contraction phase: scenarios where genetic diversity *i)* decreased throughout the contractions, *ii)* increased for periods that could be greater than thousands of years before plateauing and then decreasing or *iii)* followed a persistent increasing trend, without any visible effect of the expansion or contraction. We show that these different temporal dynamics can be predicted by comparing the observed expected heterozygosity (H_e) to the values expected if the species were at equilibrium within the refuge (H_e^{refuge}) and within the whole landscape ($H_e^{landscape}$). We also observe that there are scenarios where a rapid contraction maintains more diversity just at the end of the contraction, as widely believed and as reported in a previous simulation study. However, we also observe the opposite pattern for a wide range of parameters. The widespread idea that observing high diversity levels in a refugium population is due to a recent and rapid habitat loss is thus not necessarily true and will depend on various life history traits and how they relate to habitat change dynamics.

Introduction

The current spatial distribution of species arises from complex interactions between extrinsic (e.g., habitat and climate change) and intrinsic (e.g., dispersal) factors over various timescales, ranging from decades to tens or hundreds of millennia. Major climatic changes are thought to lead to significant changes in species distribution, leaving putative genetic signatures in the genomes of populations (Hewitt, 1996, 2004). Recently, human activities have also been altering species distributions (Finn et al., 2023), leading to range contractions (Laliberte and Ripple, 2004; Wolf and Ripple, 2017; Ceballos et al., 2017), expansions (Pacifici et al., 2020; Beyer and Manica, 2020) or fragmentation (Cushman, 2006; Haddad et al., 2015). Understanding the genetic consequences of changing habitats, population sizes and connectivity is crucial, given the central role of genetic diversity in determining a species capacity to adapt to new environmental conditions and the negative effects of inbreeding in small populations (Frankham, 2005). Investigations into the genetic effects of population size changes have a long history. For instance, both theoretical (Nei et al., 1975; Maruyama and Fuerst, 1985; Allendorf, 1986) and empirical (Cabe, 1998; Dures et al., 2019; Leigh et al., 2019) studies found that population declines reduce genetic diversity in natural populations. However, some empirical studies have also observed little to no loss (Welch et al., 2012; Maebe et al., 2016a; Crates et al., 2019) or even an increase in the genetic diversity of species experiencing population declines (Townsend et al., 2023).

The apparent disconnection between genetic diversity and contemporary population decline in a number of studies presents a significant hurdle, particularly when trying to incorporate genetic diversity into policy and conservation practices (Hoban et al., 2021; Laikre, 2010). One reason is that it remains challenging to separate and identify the contribution of major evolutionary factors such as drift, migration, mutation and life-history traits in shaping the genetic diversity of a species (De Kort et al., 2021). To investigate the evolution of genetic diversity amidst the intricate interplay of demographic and ecological factors over space and time, spatially explicit models have been particularly useful. They not only provide a better representation of natural populations but also complement, validate, or extend analytical results that are often limited to much simpler models (Edmonds et al., 2004; Klopfstein et al., 2006; Schneider et al., 2010; Rasteiro et al., 2012; Szép et al., 2022). While spatial simulations may be more difficult to interpret due to the potentially large number of parameters, they have yielded new insights into the genetics of spatial expansions (Klopfstein et al., 2006; Edmonds et al., 2004; Schneider et al., 2010) or contractions (Leblois et al., 2006; Pflüger et al., 2019; Rogan et al., 2023; Arenas et al., 2012; Sgarlata et al., 2022a) and have significantly contributed to our understanding of how spatial processes can influence the evolution and distribution of genetic diversity. However, with few exceptions (Rasteiro et al., 2012; Garnier and Lafontaine, 2022), they generally do not incorporate life-history traits into their analyses. Consequently, the extent to which genetic diversity patterns vary across different species undergoing the same habitat changes remains to be elucidated.

To address this gap, we simulated scenarios inspired by climatic oscillations of the Quaternary. During these periods, habitats and geographical ranges of species expanded from refugial areas and subsequently contracted over the glacial-interglacial periods (Hewitt, 1996; Schmitt, 2007) into two refugia. Similar refugia probably played a vital role in allowing species to survive unfavorable periods and to recolonize the landscape when conditions improved (Sommer and Nadachowski, 2006; Hewitt, 2004). We used spatial simulations and analytical derivations under a panmictic population model to investigate the temporal dynamics of genetic diversity within refugium populations. Specifically, we investigated how these dynamics were affected by a range expansion followed by a contraction, considering various contraction speeds and life-history traits. We built upon the simulation study of Arenas et al. (2012), by considering comparable habitat changes. We first focused on the effect of generation length variation and its impact on genetic diversity patterns across different scenarios of habitat changes. We then simulated habitat changes using more realistic life-history parameters, with variations such as population density, dispersal distance, and generation length, accounting for known for the reported allometric relationships of mammalian species. Our simulations allowed us to (a) describe the temporal dynamics of genetic diversity in expanding and contracting populations,

(b) pinpoint significantly different dynamics of genetic diversity trajectories as a function of life-history traits, and (c) highlight contrasting effects of contraction speeds on the patterns of genetic diversity at the end of contraction.

Materials and Methods

Simulation tool

All the simulations were performed using the in-house SINS (Simulating Individuals in Space) program. An earlier version of SINS has been used in (Rasteiro et al., 2012) whereas the latest version has been used in (Sgarlata et al., 2022a,b). SINS allows the simulation of the joint spatio-temporal evolution of both genetic and demographic data over non-overlapping discrete generations. Specifically, SINS is a population-centered but individual-based software that uses a forward-time approach to simulate diploid individuals (males and females) over a two-dimensional grid of demes, similar to a 2D stepping stone lattice (Kimura and Weiss, 1964), and along general principles inspired by SPLATCHE (Currat et al., 2004). SINS and SPLATCHE (and the subsequent SPLATCHE versions 2, 3) (Currat et al., 2004; Ray et al., 2010; Currat et al., 2019) share several features but also differ in some properties as noted in (Rasteiro et al., 2012; Sgarlata et al., 2022a,b). For instance, SINS can simulate several types of molecular markers at the same time (mtDNA, Y chromosome) and can account for variance in reproductive success, unlike SPLATCHE or its later versions. More details on the comparison between the SINS and SPLATCHE implementations can be found in (Rasteiro et al., 2012; Sgarlata et al., 2022a,b).

In SINS, each deme is characterized by its carrying capacity (K) and friction (F) values. The population size in each deme evolves using the logistic growth formula (Smith and Slatkin, 1973), corrected to account for the fact that the growth is limited by the number of reproductive females (Rasteiro et al., 2012). Therefore, the expected number of diploid individuals in generation $t+1$ is given by

$$E(N_{t+1}) = 2N_{f,t}\frac{1+r}{1+r(\frac{2N_{f,t}}{K})} \tag{1}$$

where $N_{f,t}$ is the number of females at generation t, r is the intrinsic growth rate per generation and K is the deme carrying capacity. Note that deme population size N_{t+1} is not computed deterministically as the number of individuals in generation $t+1$ is drawn from a Poisson distribution with mean $E(N_{t+1})$. We consider random mating within demes, meaning that one reproductive individual from each sex is randomly chosen to generate new offspring, which inherit one allele from each parent for each locus. At each generation, mating occurs iteratively until N_{t+1} is reached.

Each focal deme can then exchange migrants at a certain rate, with up to four neighboring demes, depending upon the geographical location of the focal deme within the available habitat boundaries. Such migrations can only occur towards demes with suitable habitat (i.e. any demes having a non-null carrying capacity, $K>0$, and friction rate strictly lower than one, $F<1$). The number of individuals migrating from the focal deme at each generation is drawn from a Poisson distribution with mean $M = \frac{N_t m n_d}{4}$, where m is the migration rate per generation and n_d is the number of available neighboring demes. The probability $P_{i,j}$ that one migrant from the focal deme i moves to a neighboring deme j depends on the friction values of all neighboring demes:

$$P_{i,j} = \frac{1-F_j}{\sum_{k\in\Gamma(i)}(1-F_k)} \tag{2}$$

where $\Gamma(i)$ denotes the set of demes in the neighborhood of deme i in the lattice. The number of migrants moving to each neighboring deme from a focal deme is sampled from a multinomial distribution with probabilities given by Eq. 2. While several types of molecular markers can be simulated,

for the current study, we exclusively used independent microsatellite loci, mutating according to the Stepwise Mutation Model (Ohta and Kimura, 1973).

Methodological details

We simulated a hypothetical landscape of 18×18 demes with two refugia of 2×2 demes each. All demes were assumed to reach the same carrying capacity (K) throughout the landscape, once colonized. For the sake of clarity, we consider that the landscape is oriented north-south, and the two refugia (Figure 1A) were located in the southeastern and southwestern corners (hereafter referred to as SE refugium and SW refugium, respectively). The simulation began with an ancestral population at the top-left deme of the 2×2 SW refugium (Figure 1A) with one allele per microsatellite (considering 50 microsatellites in total, see below). The mean number of alleles (hereafter MNA) was thus 1 and the expected heterozygosity (hereafter H_e) was 0. The size of the ancestral population was set to K, which was allowed to vary according to the simulated scenarios (Table S1). The total population size across the landscape reached the total number of demes ($18 \times 18 + 8$) times the carrying capacity K when the entire landscape was initially colonized. After the contraction phase, it decreased to $(2 \times 4) \cdot K$ (where 4 corresponds to the number of demes in each of the SW and SE refugia, Figure S3). Altogether, this corresponds to an increase of more than (and a decrease of around) two orders of magnitude of the total population size. Once the whole landscape was colonized, the overall population size ranged from $16,600$ when $K = 50$ to $332,000$ when $K = 1000$ individuals. We used a growth rate of $r = 0.8$ per generation across all simulations. We simulated 50 independent microsatellite loci per individual, with a stepwise mutation rate of 10^{-3} per locus per generation. This rate aligns with estimates reported in the literature for several mammalian species (Schlötterer et al., 1998).

While the number of generations serves as a fundamental unit of time in population genetics, habitat changes are often described in years as they more accurately reflect the temporal scale of extrinsic environmental change. This choice of describing changes in habitats in years allowed us to examine the effects of the same habitat change for multiple co-existing species with varying life-history traits. The total duration of the simulation (in years) was the same across range contraction scenarios and was set to $\simeq 14,150$ years. The number of generations spanned by habitat changes thus differed between species, depending on their respective generation length (henceforth denoted by GL).

Habitats expanded over the entire landscape over 360 years, following a series of 18 expansion steps (Figure 1B, green period). For each northward expansion step, occurring every 20 years, we created a new horizontal line of 18 demes available for colonization. Each deme was assumed to cover an area of 100×100 km^2, resulting in a landscape that extended over $1,800$ km from the southernmost to the northernmost demes. The habitat expansion speed was set at approximately 5 km/year, which is higher but comparable to the estimated rate of spread observed in European pine, hazel, and alder (estimated to be 1.5 to 2 km/year according to Hewitt (1996)). Following the expansion phase, the habitat remained stable for $2,500$ years before habitat contraction began. Throughout the stationary period, different species may colonize the landscape at varying rates, depending on their respective migration and growth rates. Except for one specific parameter combination ($GL = 10$ years, $K = 1,000$, $m = 0.003$), species with other parameter combinations colonized the entire landscape before habitat contraction began, as indicated in Table S1. To simulate habitat contraction, we set a horizontal line of 18 demes from the northern edge of the landscape as uninhabitable by setting $K = 0$ and $F = 1$. We define the onset of contraction as the time when the first line of habitats is emptied at $time = 2,860$ years. This process was then repeated at fixed time intervals, considering three durations for each contraction step: 20, 240 or 640 years. This resulted in a total duration of range contraction (hereafter t_{cont}) of 340, $4,080$, and $10,880$ years, respectively (Figure 1B). These durations of contractions correspond to contraction speeds of approximately 5.3, 0.44, and 0.16 km/year. The longer the duration of the total contraction phase, the slower the contraction speed.

Sampling design and statistics summarizing genetic diversity

To investigate the temporal dynamics of genetic diversity, we conducted 15 independent simulations for each of the scenarios depicted in Figure 1B. Specifically, we sampled 40 diploid individuals from the SW refugium, with 10 individuals selected from each of the four demes, across 60 time points. The timing of sampling (in years) remained the same for all species across scenarios with different contraction speeds. To assess the molecular diversity at the end of contraction with different speeds, we followed two sampling schemes: (i) we sampled 40 individuals from the SW refugium, selecting 10 individuals from each of its four demes, as done for the time series; and (ii) we sampled 20 individuals randomly across four demes each in both the SW and SE refugia.

We computed three summary statistics, averaged over 50 microsatellites: mean number of alleles (MNA), expected heterozygosity (H_e), and genetic differentiation among both refugia (F_{st}, Weir and Cockerham). We performed the computations of summary statistics using R software version 4.2.3 (Team et al., 2016). We calculated H_e and F_{st} using hierfstat R package (v0.5.11) (Goudet, 2005), while MNA was computed using the adegenet R package (v2.1.10) (Jombart, 2008).

Parameter selection for species: Allometric relationships

We employed allometric relationships and published data to generate biologically relevant parameter values for population density (D), mean dispersal distance (σ), and generation length (GL). Allometric relationships relate life-history traits with easily measurable traits, e.g. body mass (BM) (Peters and Peters, 1986; Blueweiss et al., 1978). Except for GL, population density, and dispersal distance can be described in the form of

$$Y = a(BM)^b \tag{3}$$

where Y represents the biological characteristic of interest, BM represents the body mass of the species, and a and b are empirically derived constants.

Allometric relationships show that body mass negatively correlates with population density and positively with dispersal distance. We used the allometric relation reported for population density and body mass (Damuth, 1981):

$$D = 68.72(BM)^{-0.75}$$

where D is population density in units of individual per km^2 and BM is body mass in grams. For dispersal distance, we used a dataset linking empirical estimates of mean dispersal distance (σ) to body mass across 164 mammal species (Santini et al., 2013). Since our simulations assume no bias in migration rate between sexes, we only used data points where dispersal distance was not sex-specific, or where the ratio in sex-specific dispersal ($max(male, female)/min(male, female)$) was less than 1.2. The resulting data points were analyzed using linear regression on a logarithmic scale obtaining the following relation

$$\sigma = 0.05(BM)^{1.26} \tag{4}$$

where σ is dispersal distance in km per generation and BM is body mass in grams. The data points between BM and σ are represented in Figure S6.

Given that no reported allometric relationship exists between GL and BM, we manually sampled nine combinations of body mass and generation length values from a public dataset on mammalian generation lengths (Pacifici et al., 2013). We considered species with body masses ranging from 0.1 kg to 100 kg because Equation 3 is only valid within this range (Silva and Downing, 1995). By visually inspecting the data represented in Figure S6A, we can distinguish two different trends:

- Species that vary in GL (1-20 years) but show little variation in BM (1-5 kg).
- Species that vary in BM (between 5-100 kg) but show little variation in GL (occurring mostly in the range of 4-10 years).

The first trend corresponds to species differing in generation lengths but which have similar population density and dispersal distances, while the second trend refers to species with similar generation lengths but varying in population density and dispersal distances. We selected three generation lengths (2, 5, 10 years) and five different body mass points (Table S1). For the chosen body masses, we used allometric relationships to compute corresponding population densities and dispersal distances.

Conversion of dispersal distances to migration rates in a stepping-stone model

Dispersal distances of species are measured in continuous space and can be related to migration rates between demes in the stepping stone model via the following equation (Baird and Santos, 2010; Al-Asadi et al., 2019)

$$\sigma^2 = mX^2$$

where σ is the root mean squared axial parent-offspring distance (dispersal distance) per generation, m is the probability that an individual from any focal deme moves to neighboring demes (migration rate) per generation and X denotes the edge length of a deme (here set as 100 km). Thus, given the dispersal distance σ, we have $m = (\frac{\sigma}{X})^2$.

Panmictic model with time-varying population size

Although the former stepping-stone framework allowed us to vary the parameters related to life-history traits, we kept certain parameters constant due to the computational cost associated with spatial simulations, for instance, the duration of the stationary phases. To better understand the results obtained from spatial simulations, we proposed a simplified panmictic population model (Nei et al., 1975) which assumes similar changes in population sizes to the ones in the spatial simulation. This panmictic model allowed us to derive the expected heterozygosity (H_e) analytically. Forward in time, we started with a population of N_i diploid individuals that were all homozygous (i.e. $H_e = 0$ or homozygosity, $F = 1$). This population immediately underwent an instantaneous population expansion to N_{exp} individuals. The population then remained stable for t_{stat} generations till the start of the contraction phase. During contraction, population size reduced linearly over a duration of t_{cont} generations, eventually reaching N_i individuals (schematized in Figure 5A). The population size changes can be summarised as:

$$N(t) = \begin{cases} N_i & \text{if} \quad t = 0 \\ N_{exp} & \text{if} \quad 0 < t \leq t_{stat} \\ N_{exp} - \left(\frac{N_{exp} - N_i}{t_{cont}}\right)(t - t_{stat}) & \text{if} \quad t_{stat} < t \leq t_{stat} + t_{cont} \\ N_i & \text{if} \quad t > t_{stat} + t_{cont} \end{cases} \tag{5}$$

To find the analytical expression for the expected heterozygosity (H_e), we utilized homozygosity $F = 1 - H_e$. The recurrence formula for the homozygosity F, defined as the probability that two alleles, randomly chosen without replacement, are identical by descent at generation t, is given by:

$$F_t = (1 - u)^2 \left\{ \frac{1}{2N_{t-1}} + \left(1 - \frac{1}{2N_{t-1}}\right) F_{t-1} \right\} \tag{6}$$

where N_{t-1} represents the size of the population at time $(t-1)$ generation and u is the mutation rate per generation.

At equilibrium, $F_t = F_{t-1}$, the expected homozygosity for a population of N individuals, denoted by $F_{eq}(N)$, reads:

$$F_{eq}(N) = \frac{(1-u)^2}{(1-u)^2 + 2N(1-(1-u)^2)} \tag{7}$$

The above equation reduces to the known form $F_{eq}(N) = \frac{1}{1+4Nu}$ for $u \ll 1$. Approximating $F(t) - F(t-1) \simeq \frac{dF}{dt}$, equation (6) reads:

$$\frac{dF}{dt} = (1-u)^2 F\left[1 - \frac{1}{2N} - \frac{1}{(1-u)^2}\right] + \frac{(1-u)^2}{2N} \tag{8}$$

The former differential equation can be solved analytically to derive an expression of F over the stationary and contraction phases.

For the stationary period ($t > 0$ to $t \leq t_{stat}$ generations), integrating equation 8 with $N = N_{exp}$ and initial condition $F(t=0) = 1$, we get (for detailed steps, refer to Supplementary S3):

$$F_{stat}(t) = F_{eq}(N_{exp}) + [1 - F_{eq}(N_{exp})]\, e^{\left[(1-u)^2\left(1-\frac{1}{2N_{exp}}-\frac{1}{(1-u)^2}\right)\right]t} \tag{9}$$

where $F_{stat}(t)$ represents the homozygosity during time interval $0 < t \leq t_{stat}$ generations and $F_{eq}(N_{exp})$ represents the equilibrium homozygosity for N_{exp} individuals.

Similarly, we can obtain the expression of the homozygosity at any time $\Delta t_{cont} = t - t_{stat}$ during the contraction phase (denoted by F_{cont}). Specifically, setting $N = N_{exp} - \left(\frac{N_{exp}-N_i}{t_{cont}}\right)(t - t_{stat})$ and $F_{cont}(0) = F_{stat}(t_{stat})$ as the initial condition, we obtain (for detailed steps, refer to Supplementary S3):

$$F_{cont}(\Delta t_{cont}) = F_{stat}(t_{stat}) e^{(a-1)\Delta t_{cont}} \left(1 - \frac{c}{b}\Delta t_{cont}\right)^{a/c} + e^{(a-1)(c\Delta t_{cont}-b)/c} \left(\frac{a}{c}\right) \left(\frac{(a-1)(c\Delta t_{cont}-b)}{c}\right)^{a/c} \left\{\Gamma\left(\frac{-a}{c}, \frac{(a-1)(c\Delta t_{cont}-b)}{c}\right) - \Gamma\left(\frac{-a}{c}, \frac{(1-a)b}{c}\right)\right\}, \tag{10}$$

where $\Gamma(s,x)$ denotes the incomplete Gamma function. Note that, we defined $\Delta t_{cont} = t - t_{stat}$, $a = (1-u)^2$, $b = 2N_{exp}$, $c = 2\left(\frac{N_{exp}-N_i}{t_{cont}}\right)(t - t_{stat})$ to ease notation.

Once contraction ends, population size remains constant ($N = N_i$). Therefore, integrating equation 8 with $N = N_i$ and initial condition $F_{cont}(t_{stat} + t_{cont})$ (homozygosity at the end of contraction), we get:

$$F_{cont-refuge}(\Delta t_{cont-refuge}) = F_{eq}(N_i) + [F_{cont}(t_{stat} + t_{cont}) - F_{eq}(N_i)]\, e^{(1-u)^2\left(1-\frac{1}{2N_i}-\frac{1}{(1-u)^2}\right)\Delta t_{cont-refuge}}, \tag{11}$$

where we have defined $\Delta t_{cont-refuge} = t - t_{stat} - t_{cont}$.

From the homozygosity values, we can express the temporal evolution of H_e as:

$$H_e(t) = \begin{cases} 0 & \text{if} \quad t = 0 \\ 1 - F_{stat}(t) & \text{if} \quad 0 < t \leq t_{stat} \\ 1 - F_{cont}(t - t_{stat}) & \text{if} \quad t_{stat} < t \leq t_{stat} + t_{cont} \\ 1 - F_{cont-refuge}(t - t_{stat} - t_{cont}) & \text{if} \quad t > t_{stat} + t_{cont} \end{cases} \tag{12}$$

The expression of H_e above is given in units of generation as time units. To account for variation in generation lengths among species, time should be rescaled as $\tilde{t} = \frac{t}{GL}$, where GL represents the generation length of the species.

Results

Temporal dynamics of genetic diversity in the refugium across different speeds of contraction

In Figure 1A, we illustrate the underlying spatial structure of our stepping-stone model, while Figure 1B depicts the expansion-contraction scenarios that were simulated onto the landscape. We assumed that species initially reside in the top-left deme of the 2×2 southwestern (SW) refugium. The habitat undergoes a sequence of phases:(i) expansion, when habitat grows northward from the SW refugium; (ii) stationary, when the habitat has filled the whole landscape; and (iii) contraction, when the habitats reduces step by step until the only habitat left is located in the two refugia. During these phases, the species colonizes new areas as a function of its intrinsic growth rate, migration rate and generation time. For most parameter combinations (eight out of nine) used here, the different species colonized the whole habitat before the contraction started. They thus experienced a stationary phase, where population size remained constant, before decreasing when habitat contracted. The three scenarios that we considered differed in the duration of the contraction phase (t_{cont}) and are represented in Figure 1B: *i)* $t_{cont} = 340$ years, *ii)* $t_{cont} = 4,080$ years, or *iii)* $t_{cont} = 10,880$ years. Once the contraction ended, the different species survived in the two SW and SE refugia until the simulation was stopped at time $14,150$ years.

Figure 2 depicts the evolution of H_e in the SW refugium for two species with generation length $GL = 0.5$ (Figure 2A) and $GL = 5$ (Figure 2B) years respectively, having the same carrying capacity ($K = 50$) and migration rates ($m = 0.2$ per generation). For both species, H_e increases during the expansion and stationary phases, though at a significantly faster pace for the species with shorter generation length. Then, H_e trajectories between the two species depart significantly during the contraction phase.

The species with shorter GL exhibits persistent H_e levels for the two long-duration contractions, plateauing before decreasing only towards the end of the contraction (Figure 2A). In contrast, species with a longer GL continue accumulating genetic diversity during the contraction phase, regardless of the contraction duration (Figure 2B). For instance, for $t_{cont} = 4,080$ years (Figure 2B, blue line), the genetic diversity of the species with $GL = 5$ years keeps increasing for over $3,000$ years (between time interval $2,860 - 6,000$ years) after habitat had started contracting (Figure 2B, black line). Overall, the species with a shorter GL shows a quicker response (in both increase and decrease of its genetic diversity) to habitat changes throughout the simulation process. Regarding the impact of contraction speed on genetic diversity, we observed that for both species, at any time point following the start of contraction, faster contraction scenarios consistently led to lower genetic diversity than slower contraction scenarios. This is expected, since at any time point during the contraction phase, faster contractions imply smaller habitat ranges and population sizes than slower contractions.

We also assessed the impact of contraction speeds on the genetic diversity at the end of contraction, following the approach in Arenas et al. (2012). Figure 3 illustrates H_e in the SW refugium population at four different time points (10, 60, 160, and 310 years), after the end of the contraction period for the three contraction speeds. For shorter GL (0.5 years, Figure 3A), the genetic diversity at the end of the fast contraction ($t_{cont} = 340$ years, red bars) is consistently greater than for the slowest contraction speed ($t_{cont} = 10,880$ years, green bars), regardless of the sampling times following the end of contraction. While the difference is statistically significant for early sampling times (10 years post end of the contraction), it diminishes as time progresses after the end of the contraction. This observation aligns with the findings reported in Arenas et al. (2012), where faster contractions were interpreted to preserve higher levels of initial genetic diversity than slower contrac-

tions. However, for a species with longer GL (5 years, Figure 3B), the opposite pattern is observed, with a higher genetic diversity at the end of the slow contraction ($t_{cont} = 10,880$ years, green bars) compared to the end of the fast contraction ($t_{cont} = 340$ years, red bars). These results are thus in contrast with those of Figure 3A and remained consistent across different combinations of carrying capacities, migration rates, and sampling schemes (see Table S3 and S4). These results suggest that depending on their life-history traits, some species may still accumulate genetic diversity during slow contraction periods (see next section).

These simulations show that variation in generation lengths alone can strongly impact the patterns of genetic diversity sampled in the refuge population during and at the end of different contraction speeds. In Figure 2, we observed that such effect seems to be related to the amount of genetic diversity accumulated in the SW refugium before the start of contraction (time $= 2,860$ years, black vertical line), with respect to the expected mutation-drift-migration equilibrium values (horizontal lines in Figure 2). Specifically, for the parameter combinations considered, these equilibria correspond to $H_e^{refuge} \simeq 0.36$ when the species is isolated in the SW refugium. Additionally, $H_e^{landscape} \simeq 0.77$ represents the value of H_e measured in the SW refugium population when the entire landscape has been colonized for extended periods. In the above simulations, at the beginning of contraction (time $= 2,860$ years), the species with $GL = 0.5$ years have $H_e \simeq 0.73$ (significantly above H_e^{refuge}, close to $H_e^{landscape}$) whereas the species with $GL = 5$ years has $H_e \simeq 0.56$ (closer to H_e^{refuge}, below $H_e^{landscape}$).

The results obtained in this first set of simulations assumed that the two simulated species differed only in their generation length, all other demographic parameters remained the same (per generation), namely carrying capacity (K), growth rate (r), and migration rate (m). Yet, real species vary not only in their generation lengths but also in other life-history traits such as population density and dispersal, and may thus exhibit patterns that differ from those reported in the present section. In the next section, we investigate the dynamics of genetic diversity for various life-history traits.

Temporal genetic diversity with allometric relations across different speeds

We investigated the H_e trajectories in our spatial framework considering three variable life-history traits (generation length, dispersal distance, and population density) which are likely to influence local and global genetic diversity. Using empirical datasets, as detailed in the Methods section, we identified demographic parameters inspired by real species allometric relationships (see Table S1 for parameter values). We found that for all considered combinations of life-history traits values in Table S1, the genetic diversity at the start of habitat contraction was always lower than their associated H_e^{refuge}, the H_e value at equilibrium when the species is isolated in the SW refugium (Figure 4). These patterns thus differ from those described in the previous section, where H_e before the start of contraction was greater than H_e^{refuge} (Figure 2).

In Figure 4, we represented the results for two species with different generation lengths, carrying capacities, and migration rates. In Figure 4B, we considered a species with $GL = 5$ years and a body mass $BM = 76.34$ kg (leading to $K = 150$ and $m = 0.059$, which aligns with species like wild goats or bush pigs). We found that the amount of H_e at the start of contraction (Figure 4B, time $= 2,860$ years, black vertical line, $H_e \simeq 0.53$) is close to H_e^{refuge} (horizontal dashed line). Then, under the slow contraction (green curve), H_e continues to increase for $8,000$ years during the contraction phase (between the time interval $4,000 - 12,000$ years), before decreasing. During the contraction phase under the fast contraction (Figure 4B, red line), H_e in the refugium increases monotonically towards H_e^{refuge} and then plateaus after the end of the contraction. Surprisingly, despite a significant loss in population size ($\simeq 98\%$ of the habitat), the trajectory of H_e for fast contraction never decreases. In contrast, H_e for slower contractions shows an initial increase above H_e^{refuge}, before decreasing during the contraction phase. Thus, for more realistic combinations of biological parameters, different contraction speeds also lead to distinct temporal trajectories of genetic diversity during the contraction phase, as observed in the previous section (Figure 2).

In Figure 4C, we considered a species with $GL = 10$ years and $BM = 6.09$ kg (leading to

$K = 1,000$ and $m = 0.003$, characteristic of species like lion-tailed macaque). In this case, the amount of genetic diversity at the beginning of contraction (time $= 2,860$ years) is significantly lower than H_e^{refuge}. The duration of the contraction phase was such that the genetic diversity remained below H_e^{refuge}, regardless of the contraction speeds considered. We observed little to no differences in H_e across contraction speeds (Figure 4C). This similarity in trajectories arises because genetic diversity in the refugium population is increasing towards H_e^{refuge} and keeps on accumulating genetic diversity within the refugium, despite the fact that the species as a whole loses a large amount of population size across the landscape. The habitat changes outside of the refugium areas therefore have a negligible effect on the genetic diversity observed in the refugium.

Panmictic model of range contraction: analytic solutions

The computational demands of spatial simulations constrained the amount of variable parameters that could be tested, thereby limiting the generality of conclusions that could be made regarding the genetic signatures of habitat change. To overcome this limitation and generalize our findings for a wider range of scenarios and life-history traits, we considered a simplified panmictic model where the temporal evolution of H_e could be solved analytically (cf. Materials and Methods section). The panmictic model represents a single population experiencing similar but simplified dynamics of habitat change (here modeled as effective population size variations, Figure 5A). Specifically, we assumed an initial population of N_i genetically homogeneous individuals ($H_e = 0$). This population underwent an instantaneous expansion to N_{exp} individuals and remained stable for t_{stat} generations. Afterward, the population size contracted back to N_i, linearly over t_{cont} generations.

Figure 5B illustrates distinct temporal dynamics of genetic diversity during the contraction phase for a stationary duration of $1,000$ generations and a contraction phase of 800 generations. Varying N_i and N_{exp} influenced the mutation-drift equilibrium values ($H_{eq}^{N_i} = H_e^{refuge}$ and $H_{eq}^{N_{exp}} = H_e^{landscape}$), leading to different temporal dynamics of genetic diversity as the ones observed in the refugium population from the previous spatial simulations. In particular, our panmictic model could reproduce the same temporal dynamics of genetic diversity as the ones observed in the SW population from the previous spatial framework.

Lastly, we analyzed the impact of varying generation length on patterns of genetic diversity at the end of contraction by varying the stationary (t_{stat}) and contraction (t_{cont}) durations in our panmictic model, using equation 12 and assuming $N_i = 100$, $N_{exp} = 10^4$ and $u = 0.001$. We represent in Figure 5C the variations of H_e at the end of contraction, as a function of the contraction and stationary times. Our results are qualitatively similar to those observed for the spatial simulations. For instance, considering a stationary phase of $1,250$ years, this duration would translate into $t_{stat} = 2,500$ ($t_{stat} = 250$) generations for a species with $GL = 0.5$ ($GL = 5$) years before habitat contraction starts. These two species will experience different trajectories of H_e, qualitatively similar to those represented in the first two panels of Figure 5B.

Figure 5D shows how H_e values differ at the end of contraction between both species, in a similar way comparable to Figure 3. For $t_{stat} = 2,500$ generations (short $GL = 0.5$ years, black horizontal line in Figure 5C and black curve in Figure 5D), there is enough time for H_e to reach the mutation-drift equilibrium ($H_e^{N_{exp}}$) before the contraction starts. Consequently, genetic diversity at the end of contraction decreases as contraction duration increases. Thus, H_e at the end of faster contractions is higher than at the end of slower ones. This finding aligns with the results obtained from spatial simulations conducted with the species having $GL = 0.5$ year (see Figure 3A) and with (Arenas et al., 2012). Conversely, for the species with long $GL = 5$ years, the population is far from the equilibrium value $H_e^{N_{exp}}$ at the start of habitat contraction. Therefore, for $t_{stat} = 250$ generations (grey horizontal line in Figure 5C and grey curve in Figure 5D), we observe that H_e at the end of contraction increases as contraction time increases (slower contractions maintain more diversity) till $t_{cont} \approx 1,000$ generations. This is in agreement with the spatial simulation for $GL = 5$ years (Figure 3B) where we found higher genetic diversity at the end of slow contraction compared to fast. However, the panmictic model predicts that H_e starts to decrease as

the contraction time is further increased (Figure 5D, grey curve, when $t_{cont} > 1,000$ generations), resulting in an overall non-monotonous trajectory for H_e. The two types of relationships we observe for H_e at the end of contraction and contraction speed are distinguished by the amount of genetic diversity accumulated before the start of the contraction phase. In the current case, the boundary between both behaviors corresponds to $t_{stat} \simeq 1,220$ generations. In general, for $t_{stat} > 1,220$, the dependence is monotonous, whereas for $t_{stat} < 1,220$ generations the dependence is non-monotonous. For a stationary time of $1,220$ generations, the panmictic population reaches $H_e = 0.896$, which is approximately $\simeq$90% of the equilibrium value of genetic diversity of the expanded population size (N_{exp}).

The non-monotonic trend between H_e at the end of contraction and t_{cont} identified under the panmictic model was not observed in the spatial simulations due to the limited duration of the range contractions that were tested. To overcome this limitation, we conducted additional spatial simulations, considering longer contraction times. Figure 5E confirms that H_e eventually decreases for longer contraction times, giving rise to the non-monotonic trend predicted by the panmictic model. These results are further supported when analyzing the dependence of MNA at the end of the contraction, as represented in Supplementary Figure S7.

Discussion

Natural populations undergo changes in population size and geographical distribution across various spatial and temporal scales. As a result, many species are likely to deviate from mutation-migration-drift equilibrium due to many (non-exclusive) factors, including fluctuations in habitat availability, variation in life-history traits, and dispersal patterns, as a consequence of geographical or environmental barriers. Here, we explored the idea that life-history traits could greatly influence our expectations of the genetic consequences of habitat changes. We investigated the temporal dynamics of genetic diversity (as measured through the expected heterozygosity, H_e, and the mean number of alleles, MNA) in a refugium population subjected to a range expansion and subsequent contraction. We used spatially explicit individual-based simulations and analytical results from a panmictic single population model. Our analyses revealed that generation length significantly impacted the dynamics of genetic diversity. Further, the interaction between generation length, carrying capacity, and dispersal rate with the speed of habitat changes led to contrasting trajectories of genetic diversity between species experiencing the same scenario of habitat change. We explored different parameter combinations, and identified three distinct temporal dynamics of H_e and MNA in the refugium population: (i) an initial increase followed by a continuous decrease, starting when habitat starts contracting; or (ii) an increase that continues for a very long period after habitat started contracting, followed by a delayed decrease; or (iii) a continuous increase during the whole expansion and contraction period, as if habitat range had never changed beyond the refugium.

We also observed two contrasting patterns regarding the effect of contraction speed on the level of genetic diversity sampled at the end of contraction. The first pattern has already been described in spatial simulations and suggests that quick contractions maintain higher levels of diversity compared to slow contraction scenarios (Arenas et al., 2012). Thus, high diversity levels estimated in a refugium or an isolated population are often interpreted as resulting from recent habitat loss (Wang et al., 2022). The second pattern is characterized by non-monotonicity of H_e (estimated at the end of contraction) with respect to the speed of contraction: quick contractions maintain less genetic diversity than slower contractions up to a certain contraction speed. Beyond this threshold speed, the trend reverses as contraction speed reduces (Figure 5D, E). In other words, fast and slow contraction speeds maintain less genetic diversity (at the end of the respective contraction phases) than intermediate speeds. Under such scenarios, observing high diversity in a refugium, after habitat contraction, does not necessarily reflect a recent habitat loss.

Altogether, our spatial and panmictic analysis allowed us to identify different temporal trajectories between population size, genetic diversity, and contemporary habitat extent, hence questioning our ability to accurately infer habitat extent or population size from patterns of genetic diversity.

More specifically, our results suggest that the increasing use of genetic data to reconstruct the demographic history of species (interpreted as changes in effective population size, N_e) may not be straightforwardly connected to ancient habitats and population sizes. Our work also emphasizes the importance and relevance of demographic inferences based on simulations, to better account for the impact of life-history traits on patterns of genetic evolution. In the next sections, we try to discuss and clarify some consequences of our work.

Temporal trajectories of genetic diversity in contracting populations

Population genetics theory states that a decrease in effective population size (N_e) leads to a reduction in genetic diversity in a panmictic model (H_e and MNA). Under simplifying assumptions, N_e is also thought to be positively correlated with census population size (N_c), which is itself correlated to the geographical range, and possibly to habitat extent (if no major barriers to gene flow are present in the range). Thus, a decline in N_c or habitat range is expected to lead to a reduction in genetic diversity, and to a decrease in N_e. These predictions find solid support in numerous empirical studies that have reported a loss of genetic diversity in species undergoing habitat loss (Nyström et al., 2006; Dures et al., 2019; Taron et al., 2021; Gauthier et al., 2020). However, several recent studies have observed no apparent reduction in genetic diversity despite drastic decreases in population sizes (Maebe et al., 2016b; Le Gouar et al., 2009; Fourcade et al., 2020; Carvalho et al., 2019), and in some cases, even an increase in genetic diversity over time has been documented (Townsend et al., 2023). These observations have been attributed to either the immigration of individuals from neighboring populations compensating for the diversity loss due to population decline or to species-specific life-history traits, such as generation time, which could delay the genetic response (Goossens et al., 2005; Hailer et al., 2006). Our results show that H_e trajectories exhibiting opposite trends with respect to population size and habitat trajectories are expected and may happen under reasonable conditions. For instance, we found that populations that deviate from mutation-drift-migration equilibrium at the start of a contraction phase can present these unexpected temporal dynamics of increasing genetic diversity over hundreds or thousands of years in the refugium population when habitats and population range are contracting. Importantly, we found that these trajectories can be predicted, by comparing the current genetic diversity of the population (*e.g.* H_e) with the genetic diversity expected under expanded and contracted habitat ranges (*i.e.* $H_e^{landscape}$ and H_e^{refuge}, respectively). Specifically, the temporal trajectory of H_e in the refugium population depends on which of the following three situations is observed at the start of contraction: (i) $H_e \simeq H_e^{landscape}$ (ii) $H_e^{landscape} > H_e > H_e^{refuge}$ (iii) $H_e < H_e^{refuge}$.

In the first regime ($H_e \simeq H_e^{landscape}$, as in Figure 2A, 5B1), the whole population is at its mutation-drift-migration equilibrium before contraction starts. Any decline in population size thus results in a decrease in genetic diversity eventually reaching the equilibrium of the refugium population size (H_e^{refuge}). If the population decline occurs at different speeds, genetic diversity at the end of faster contraction speeds is higher than that at the end of slower contractions. This is because, when contractions occur quickly, a substantial amount of genetic diversity is still retained at the end of contraction, even if it is subsequently lost rapidly. On the contrary, during slower contractions, the refugium population is subjected to more genetic drift, leading to a greater and gradual loss of genetic diversity by the end of contraction.

For the second regime ($H_e^{landscape} > H_e > H_e^{refuge}$, when contraction starts), as in Figure 2B), we find that during slower contractions, genetic diversity can keep increasing for rather long periods during contraction phase, before decreasing. A larger difference between $H_e^{landscape}$ and H_e, indicated as ΔH_e, at the beginning of the contraction phase, is associated with a longer period during which genetic diversity increases before starting to decrease. Here, fast range contractions do not preserve higher levels of genetic diversity when comparing samples at the end of slower contraction speeds. Instead, intermediate contraction speeds preserve a larger amount of genetic diversity compared to fast and slow contraction speeds (see Figure 5D, E, Figure S7). This means that, under this regime, low levels of genetic diversity in a refugium at present could be either due to a recent or ancient contraction.

Lastly, in the third regime ($H_e < H_e^{refuge}$, when the contraction starts), H_e will increase until it eventually reaches H_e^{refuge} and, if by that time the contraction is finished, H_e will stay at this level until further habitat change occurs. Under such a scenario, we will thus observe a counter-intuitive increase of diversity in refugium populations through time despite a major decrease in census population size and habitat across the landscape. However, if the contraction is very slow, such that at some point during contraction $H_e > H_e^{refuge}$, then the temporal dynamics will be similar to the second regime.

The identification of genetic diversity trajectories during population contraction has importance from a conservation point of view. Our results show that these trajectories could be identified by calculation of three quantities, H_e, H_e^{refuge}, and $H_e^{landscape}$, and knowing fundamental life-history traits. What our results also show is that spatial processes combined with variable life-history traits can generate patterns and temporal trajectories that go against a number of predictions made in theoretical or empirical studies ignoring these factors. Furthermore, closely related species undergoing similar habitat changes may exhibit divergent temporal dynamics in genetic diversity due to variations in the initial levels of genetic diversity before the habitat changes. As a consequence, this questions our ability to link N_e trajectories inferred from genetic data to ancient habitat changes, as we will discuss in the next section.

Coupling between genetic diversity, life-history traits, habitat change and demographic history

While species genetic diversity and spatial distribution are influenced by habitat changes over time (Hewitt, 2004; Svenning et al., 2015), we rarely have a direct measure of these changes. In the past few decades, population geneticists have used genetic data and sophisticated statistical methods to reconstruct the demographic history of populations or species. This "demographic history" is often implicitly or explicitly interpreted in terms of changes in N_e, which are then related to putative changes in climate or habitat (Nadachowska-Brzyska et al., 2015; Natesh et al., 2020; Teixeira et al., 2021). Yet, the idea that inferred N_e trajectories do not necessarily reflect changes in census population size (and by extension, in habitat range) has been around for some time (Wakeley, 1999; Mazet et al., 2016; Leonardi et al., 2021). Over the last two decades, an increasing number of studies have shown that statistical methods that infer N_e while ignoring population structure may infer, quantify, and date with great precision changes in N_e that never occurred (Chikhi et al., 2010, 2018). This is because structured population models have genealogical properties that can be interpreted erroneously under panmictic models (Herbots, 1994; Notohara, 1990; Wakeley, 1999; Chikhi et al., 2010; Mazet et al., 2016).

Also, co-distributed species living in the same habitat are often expected to exhibit similar demographic responses to habitat changes. As a result, it is anticipated that co-distributed species will show congruence in their genetic diversity trajectories and, consequently, in their inferred N_e. However, empirical studies suggest that such congruence is rarely observed. For example, studies inferring N_e across various taxa have reported discordant or asynchronous demographic responses to Pleistocene climate changes (Burbrink et al., 2016; Kuhn et al., 2022; Walton et al., 2021; Bai et al., 2018). Additionally, even closely related species sharing similar ecological or life-history traits may exhibit incongruent demographic histories in similar environments (Bai et al., 2018; Walton et al., 2021; Kuhn et al., 2022).

In the context of our simulated scenarios, we tested whether coalescent-based approaches to infer N_e, such as the method of Nikolic and Chevalet (2014) implemented in the R package `VarEff` would help us better elucidate the relationships between N_c, H_e, and inferred N_e trajectories. This method utilizes microsatellites to infer changes in N_e. It has been thoroughly tested and has been applied to various endangered species (Salmona et al., 2017; Srinivas and Jhala, 2023). Our goal was to assess if the various simulated scenarios, involving species with varying life-history traits undergoing similar changes in habitat, would exhibit comparable inferred changes in N_e. Additionally, we explored the ability to distinguish fast and slow contractions using inferred N_e trajectories. We conducted

the analysis using genetic data sampled at time = 14,000 years forward (end of simulation) across various contraction durations and life-history parameters (for details refer to Supplementary S6). We plotted for each of the scenarios the temporal trajectories of N_c, H_e, and inferred N_e (Figure S8). Our results suggest that the inferred N_e trajectories are not generally consistent with the simulated N_c changes, and can have variable similarity with H_e trajectories. Fast and slow contraction scenarios appear to lead to distinguishable inferred N_e trajectories. For instance, for three scenarios, the slow contraction exhibits higher inferred N_e compared to the fast contraction scenarios (Figure S8b, c, d). However, we note that in Figure S8a, the inferred N_e of fast contraction was surprisingly higher than for the slower contraction. This is surprising, as fast contraction experiences a greater loss in genetic diversity while population size remained limited to the SW refugium for a longer duration till the present. We further provide a detailed discussion in Supplementary S6. In particular, it appears that this output of the `VarEff` method, which is used to represent changes in N_e should be interpreted with care as the posterior distribution may be rather wide (Supplementary Figure S15). However, even assuming that the represented N_e trajectories should not be interpreted directly, it suggests then that the N_e trajectories cannot be used to understand past N_c or H_e trajectories or habitat extent, for the scenarios simulated here.

In fact, we stress that these results are admittedly limited to a few scenarios, suggesting that the inferred N_e trajectories that are typically used to represent the "demographic history" of species might still be acceptable as proxies for N_c under other scenarios, yet to be identified. However, here they should be taken with a grain of salt, as they may provide little information about N_c and H_e changes. These results show that inferred N_e trajectories obtained for many species are not necessarily expected to correlate with the trajectory of changes in N_c or habitat range. Furthermore, what we show is that the observed discordance in inferred N_e across multi-species studies in similar environments is not surprising but rather expected, potentially arising from differences in life-history traits. These inconsistencies are further supported by empirical studies. For example, a study by Miller et al. (2021) used a Bayesian Skyline Plot (BSP) to infer N_e and employed Species Distribution Modelling (SDM) to reconstruct the geographical range of 102 Holarctic bird species. The study revealed no correlation between the magnitude of changes in N_e and range size inferred using species distribution modeling and past climate reconstructions. We note also that BSP is known to be influenced by population structure (Heller et al., 2013). Thus disagreements between inferred N_e trajectories and inferred range size changes could also stem from variable levels of unaccounted population structure, reasons that are related to, but different from those studied here.

The problematic meaning of "demographic history" for panmictic vs. structured populations

The field of population genetics has historically relied on simple models to capture the properties of natural populations. The panmictic model, widely used for its simplicity and mathematical tractability, has proven valuable in numerous scenarios. We found that it was useful here too, since it allowed us to explore a large spectrum of parameters, identifying H_e trajectories that would have otherwise been difficult and computationally intensive to explore with spatial simulations (e.g., non-monotonic relationship between contraction duration and H_e estimated at the end of the contraction). In this study, the panmictic and spatially structured population approaches yielded consistent qualitative results regarding the temporal dynamics of H_e and the influence of contraction speed on H_e at the end of contraction. This is also because migration rates were kept constant in space and time in our spatial models. However, natural populations are generally spatially structured and have thus different properties. For instance, they typically require a larger number of generations to reach mutation-drift-migration equilibrium compared to panmictic populations (Leblois et al., 2006). As a result, spatial and panmictic populations may exhibit different temporal dynamics of genetic diversity for given population size changes (Figure S5). Our panmictic model was both useful and limited since it could not include the effect of migration, even though the latter plays a major role in the temporal decoupling of the different trajectories (N_c, H_e, N_e).

In terms of inference, the coalescent theory provides a convenient theoretical framework to link

genomic diversity with past demography. Panmictic population models are simpler to handle and simulate under a coalescent framework, making demographic inference possible and simple since only one parameter is allowed to change (N_e). Structured models are more difficult to use for various reasons. They are computationally more demanding and are also not trivially defined given the infinitely large number of model types and parameter space. Continent-island, n-island, or stepping-stone models are just a small part of the possible models, yet they can have very different properties (e.g. Chikhi et al. (2018)). However, what becomes increasingly clear is that interpreting the past demography of a species using reconstructed N_e trajectories under a panmictic model is likely to lead to misinterpretations of the past demographic history if, in reality, the populations analyzed evolved under a set of interconnected populations. An important conclusion from several published studies is that the concept of "demographic history" is problematic because it is usually interpreted in terms of changes in N_e when there are reasons to think that the concept of N_e is unclear under structured models (Chikhi et al., 2018). Here, we went further and studied a dynamic model of population structure where the population size and habitat extent both changed by at least two orders of magnitude and found that we would not have been able to say something informative about the real demographic history of our species if we had used an inferred N_e trajectory to represent the "demographic history". Following Chikhi et al. (2018), such trajectories should thus be seen as estimates of complex summary statistics, rather than objects that can be interpreted directly.

Our work suggests that, since the trajectories of N_c, habitat size, H_e, and inferred N_e cannot be expected to be coupled temporally in a simple way, they should be seen as representing different conceptual objects. Hence, the demographic history reconstructed with piecewise coalescent-based methods, such as `VarEff, PSMC, MSMC, MSMC2` or the `Stairway plot`, should be interpreted with extreme caution and be validated with simulations under structured models. Moreover, considering that co-distributed species are likely to differ in life-history traits relevant to genetics, the application of the same demogenomic inference methodology is unlikely to provide the same trajectories across species, even if they underwent similar climatic and habitat changes. Spatially explicit models remain thus necessary and valuable for assessing the genetic effects of habitat loss and fragmentation, over both short and long time scales.

Perspectives

Our results suggest that more work is needed to improve our understanding of spatially structured models undergoing cycles of expansion and contraction. We found connections between some life-history traits, H_e, and N_c dynamics, and identified potentially serious issues in the use of N_e as a proxy for any of these. We showed how comparing current H_e to H_e^{refuge} and $H_e^{landscape}$ can be used to predict the future trajectory of H_e with important implications for the conservation of endangered species currently experiencing habitat contraction (within or outside refugia). Although we simulated different species by taking into account empirical allometric relationships, we still made some simplifying assumptions. For instance, we considered homogeneous carrying capacities, migration, mutation, and growth rates. We also assumed random mating within demes for all species across the landscape and considered co-distributed species as ecologically independent, with no consideration for species interactions. Deviations from these factors could impact the time to mutation-migration-drift equilibrium and would affect the temporal scale of the genetic responses we identified here. Among many other factors, social structure is one that we consider to be relatively understudied within spatial models (Chesser, 1991a,b; Sugg et al., 1996; Parreira and Chikhi, 2015). We also assumed that the connectivity between the refugium and the neighboring populations remained similar throughout the simulation. Also, the species we simulated have non-overlapping generations but theoretical studies show that overlapping generations increase the time to reach equilibrium (Lloyd et al., 2013). Incorporating non-overlapping generations could increase the lag effect identified here, disconnecting, even more, the temporal trajectories of habitat, N_c and H_e.

Regarding our simulated scenarios, we considered specific initial conditions where all individuals were homozygous and we focused on a single cycle of range expansion and contraction, although most species likely experienced multiple glacial cycles during the Holocene and Pleistocene. Our

results indicate that the latter two limitations should not impact the main conclusions of our work, because we can still predict the behavior of the trajectories as a function of the amount of genetic diversity accumulated before a new cycle of expansion and contraction, forward in time. Yet, an interesting perspective would be to investigate the impact of multiple cycles while accounting for multiple refugia scenarios. Indeed, independent refugia can maintain divergent alleles or haplotypes for longer periods of cyclic expansions and contractions, which can complexify the trajectories of H_e and inferred N_e when these alleles mix during population reconnections. A natural extension of our work will be to explore the temporal dynamics of genetic diversity in samples from other regions within the landscape as the dynamics of their genetic diversity could be different from the ones observed within the present-day refugium. Future research should also investigate more complex patterns of range contraction (Rogan et al., 2023) and behaviors in continuous space (Leblois et al., 2006; Bradburd and Ralph, 2019).

Acknowledgements

We thank all the members of the Population and Conservation Genetic group at Instituto Gulbenkian de Ciência (IGC) for their support and useful discussions on this topic. We would also like to acknowledge the Bioinformatics Unit and the Informatics Team of the IGC for their help and support with computational resources. We acknowledge the financial support received from the Fundação para a Ciência e Tecnologia through a PhD fellowship awarded to RV (reference number: UI/BD/154372/2022), a grant awarded to GMS (PD/BD/114343/2016), and LC (PTDC-BIA-EVL/30815/2017), as well as the financial support provided by the Calouste Gulbenkian Foundation through the PONTE program to DSP. LC's research was also supported by the 2015-2016 BiodivERsA COFUND call for research proposals, with national funders ANR (ANR-16-EBI3-0014) and the Fundação para a Ciência e Tecnologia (reference: Biodiversa/0003/2015 and PT-DLR 01LC1617A). LC additionally received support from the DevOCGen project, funded by the Occitanie Regional Council's "Key challenges BiodivOc" program. This work was also supported by the LABEX entitled TULIP (ANR-10-558 LABX-41 and ANR-11-IDEX-0002-02) as well as the IRP BEEG-B (International Research Project Bioinformatics, Ecology, Evolution, Genomics and Behaviour). We acknowledge an Investissement d'Avenir grant of the Agence Nationale de la Recherche (CEBA: ANR-10-LABX-25-01).

References

Al-Asadi, H., Petkova, D., Stephens, M., and Novembre, J. (2019). Estimating recent migration and population-size surfaces. *PLoS genetics*, 15(1):e1007908.

Allendorf, F. W. (1986). Genetic drift and the loss of alleles versus heterozygosity. *Zoo biology*, 5(2):181–190.

Arenas, M., Ray, N., Currat, M., and Excoffier, L. (2012). Consequences of range contractions and range shifts on molecular diversity. *Molecular biology and evolution*, 29(1):207–218.

Bai, W.-N., Yan, P.-C., Zhang, B.-W., Woeste, K. E., Lin, K., and Zhang, D.-Y. (2018). Demographically idiosyncratic responses to climate change and rapid pleistocene diversification of the walnut genus juglans (juglandaceae) revealed by whole-genome sequences. *New Phytologist*, 217(4):1726–1736.

Baird, S. J. and Santos, F. (2010). Monte carlo integration over stepping stone models for spatial genetic inference using approximate bayesian computation. *Molecular ecology resources*, 10(5):873–885.

Beaumont, M. A. (2004). Recent developments in genetic data analysis: what can they tell us about human demographic history? *Heredity*, 92(5):365–379.

Beyer, R. M. and Manica, A. (2020). Historical and projected future range sizes of the world's mammals, birds, and amphibians. *Nature Communications*, 11(1):5633.

Blueweiss, L., Fox, H., Kudzma, V., Nakashima, D., Peters, R., and Sams, S. (1978). Relationships between body size and some life history parameters. *Oecologia*, pages 257–272.

Bradburd, G. S. and Ralph, P. L. (2019). Spatial population genetics: it's about time. *Annual Review of Ecology, Evolution, and Systematics*, 50:427–449.

Burbrink, F. T., Chan, Y. L., Myers, E. A., Ruane, S., Smith, B. T., and Hickerson, M. J. (2016). Asynchronous demographic responses to pleistocene climate change in eastern nearctic vertebrates. *Ecology Letters*, 19(12):1457–1467.

Cabe, P. R. (1998). The effects of founding bottlenecks on genetic variation in the european starling (sturnus vulgaris) in north america. *Heredity*, 80(4):519–525.

Carvalho, C. S., Lanes, É. C., Silva, A. R., Caldeira, C. F., Carvalho-Filho, N., Gastauer, M., Imperatriz-Fonseca, V. L., Nascimento Júnior, W., Oliveira, G., Siqueira, J. O., et al. (2019). Habitat loss does not always entail negative genetic consequences. *Frontiers in Genetics*, 10:1011.

Ceballos, G., Ehrlich, P. R., and Dirzo, R. (2017). Biological annihilation via the ongoing sixth mass extinction signaled by vertebrate population losses and declines. *Proceedings of the national academy of sciences*, 114(30):E6089–E6096.

Chesser, R. K. (1991a). Gene Diversity and Female Philopatry. *Genetics*, 127:437–447.

Chesser, R. K. (1991b). Influence of gene flow and breeding tactics on gene diversity within populations. *Genetics*, 129(2):573–583.

Chikhi, L., Rodríguez, W., Grusea, S., Santos, P., Boitard, S., and Mazet, O. (2018). The iicr (inverse instantaneous coalescence rate) as a summary of genomic diversity: insights into demographic inference and model choice. *Heredity*, 120(1):13–24.

Chikhi, L., Sousa, V. C., Luisi, P., Goossens, B., and Beaumont, M. A. (2010). The confounding effects of population structure, genetic diversity and the sampling scheme on the detection and quantification of population size changes. *Genetics*, 186(3):983–995.

Crates, R., Olah, G., Adamski, M., Aitken, N., Banks, S., Ingwersen, D., Ranjard, L., Rayner, L., Stojanovic, D., Suchan, T., et al. (2019). Genomic impact of severe population decline in a nomadic songbird. *PLoS One*, 14(10):e0223953.

Currat, M., Arenas, M., Quilodran, C. S., Excoffier, L., and Ray, N. (2019). Splatche3: simulation of serial genetic data under spatially explicit evolutionary scenarios including long-distance dispersal. *Bioinformatics*, 35(21):4480–4483.

Currat, M., Ray, N., and Excoffier, L. (2004). Splatche: a program to simulate genetic diversity taking into account environmental heterogeneity. *Molecular Ecology Notes*, 4(1):139–142.

Cushman, S. A. (2006). Effects of habitat loss and fragmentation on amphibians: a review and prospectus. *Biological conservation*, 128(2):231–240.

Damuth, J. (1981). Population density and body size in mammals. *Nature*, 290:699–700.

De Kort, H., Prunier, J. G., Ducatez, S., Honnay, O., Baguette, M., Stevens, V. M., and Blanchet, S. (2021). Life history, climate and biogeography interactively affect worldwide genetic diversity of plant and animal populations. *Nature communications*, 12(1):516.

Dures, S. G., Carbone, C., Loveridge, A. J., Maude, G., Midlane, N., Aschenborn, O., and Gottelli, D. (2019). A century of decline: Loss of genetic diversity in a southern african lion-conservation stronghold. *Diversity and distributions*, 25(6):870–879.

Edmonds, C. A., Lillie, A. S., and Cavalli-Sforza, L. L. (2004). Mutations arising in the wave front of an expanding population. *Proceedings of the National Academy of Sciences*, 101(4):975–979.

Finn, C., Grattarola, F., and Pincheira-Donoso, D. (2023). More losers than winners: investigating anthropocene defaunation through the diversity of population trends. *Biological Reviews*.

Fourcade, Y., Richardson, D. S., and Secondi, J. (2020). No evidence for a loss of genetic diversity despite a strong decline in size of a european population of the corncrake crex crex. *Bird conservation international*, 30(2):260–266.

Frankham, R. (2005). Genetics and extinction. *Biological conservation*, 126(2):131–140.

Garnier, J. and Lafontaine, P. (2022). Life history traits and dispersal shape neutral genetic diversity in metapopulations. *Journal of Mathematical Biology*, 84(6):45.

Gauthier, J., Pajkovic, M., Neuenschwander, S., Kaila, L., Schmid, S., Orlando, L., and Alvarez, N. (2020). Museomics identifies genetic erosion in two butterfly species across the 20th century in finland. *Molecular Ecology Resources*, 20(5):1191–1205.

Gonçalves, M., Siegismund, H. R., van Vuuren, B. J., Ferrand, N., and Godinho, R. (2021). Evolutionary history of the roan antelope across its african range. *Journal of Biogeography*, 48(11):2812–2827.

Goossens, B., Chikhi, L., Jalil, M., Ancrenaz, M., Lackman-Ancerenaz, I., Mohamed, M., Andau, P., and Bruford, M. W. (2005). Patterns of genetic diversity and migration in increasingly fragmented and declining orang-utan (pongo pygmaeus) populations from sabah, malaysia. *Molecular Ecology*, 14(2):441–456.

Goudet, J. (2005). Hierfstat, a package for r to compute and test hierarchical f-statistics. *Molecular ecology notes*, 5(1):184–186.

Grant, W. S. and Cheng, W. (2012). Incorporating deep and shallow components of genetic structure into the management of alaskan red king crab. *Evolutionary Applications*, 5(8):820–837.

Grant, W. S., Liu, M., Gao, T., and Yanagimoto, T. (2012). Limits of bayesian skyline plot analysis of mtdna sequences to infer historical demographies in pacific herring (and other species). *Molecular phylogenetics and evolution*, 65(1):203–212.

Haddad, N. M., Brudvig, L. A., Clobert, J., Davies, K. F., Gonzalez, A., Holt, R. D., Lovejoy, T. E., Sexton, J. O., Austin, M. P., Collins, C. D., et al. (2015). Habitat fragmentation and its lasting impact on earth's ecosystems. *Science advances*, 1(2):e1500052.

Hailer, F., Helander, B., Folkestad, A. O., Ganusevich, S. A., Garstad, S., Hauff, P., Koren, C., Nygård, T., Volke, V., Vila, C., et al. (2006). Bottlenecked but long-lived: high genetic diversity retained in white-tailed eagles upon recovery from population decline. *Biology letters*, 2(2):316–319.

Heller, R., Chikhi, L., and Siegismund, H. R. (2013). The confounding effect of population structure on bayesian skyline plot inferences of demographic history. *PloS one*, 8(5):e62992.

Herbots, H. M. J. D. (1994). *Stochastic models in population genetics: genealogy and genetic differentiation in structured populations*. PhD thesis, Queen Mary University of London.

Hewitt, G. M. (1996). Some genetic consequences of ice ages, and their role in divergence and speciation. *Biological journal of the Linnean Society*, 58(3):247–276.

Hewitt, G. M. (2004). Genetic consequences of climatic oscillations in the quaternary. *Philosophical Transactions of the Royal Society of London. Series B: Biological Sciences*, 359(1442):183–195.

Hoban, S., Campbell, C. D., da Silva, J. M., Ekblom, R., Funk, W. C., Garner, B. A., Godoy, J. A., Kershaw, F., MacDonald, A. J., Mergeay, J., et al. (2021). Genetic diversity is considered important but interpreted narrowly in country reports to the convention on biological diversity: Current actions and indicators are insufficient. *Biological Conservation*, 261:109233.

Hudson, R. R. (1983). Properties of a neutral allele model with intragenic recombination. *Theoretical population biology*, 23(2):183–201.

Jombart, T. (2008). adegenet: a r package for the multivariate analysis of genetic markers. *Bioinformatics*, 24(11):1403–1405.

Kimura, M. and Weiss, G. H. (1964). The stepping stone model of population structure and the decrease of genetic correlation with distance. *Genetics*, 49(4):561.

Kingman, J. F. C. (1982). The coalescent. *Stochastic processes and their applications*, 13(3):235–248.

826 Klopfstein, S., Currat, M., and Excoffier, L. (2006). The fate of mutations surfing on the wave of a
827 range expansion. *Molecular biology and evolution*, 23(3):482–490.

828 Kuhn, A., Gehara, M., Andrianarimalala, M. S., Rabibisoa, N., Randriamahatantsoa, B., Overcast,
829 I., Raxworthy, C. J., Ruane, S., and Burbrink, F. T. (2022). Drivers of unique and asynchronous
830 population dynamics in malagasy herpetofauna. *Journal of Biogeography*, 49(4):600–616.

831 Laikre, L. (2010). Genetic diversity is overlooked in international conservation policy implementa-
832 tion. *Conservation Genetics*, 11:349–354.

833 Laliberte, A. S. and Ripple, W. J. (2004). Range contractions of north american carnivores and
834 ungulates. *BioScience*, 54(2):123–138.

835 Le Gouar, P. J., Vallet, D., David, L., Bermejo, M., Gatti, S., Levréro, F., Petit, E. J., and Mé-
836 nard, N. (2009). How ebola impacts genetics of western lowland gorilla populations. *PLoS One*,
837 4(12):e8375.

838 Leblois, R., Estoup, A., and Streiff, R. (2006). Genetics of recent habitat contraction and reduction
839 in population size: does isolation by distance matter? *Molecular Ecology*, 15(12):3601–3615.

840 Leigh, D. M., Hendry, A. P., Vázquez-Domínguez, E., and Friesen, V. L. (2019). Estimated six
841 per cent loss of genetic variation in wild populations since the industrial revolution. *Evolutionary*
842 *applications*, 12(8):1505–1512.

843 Leonardi, M., Barbujani, G., and Manica, A. (2021). *Genetic demography: What does it mean and*
844 *how to interpret it, with a case study on the Neolithic transition*, page 91–100. Kerns Verlag.

845 LLC, W. A. (2009). Wolfram| alpha.

846 Lloyd, M. W., Campbell, L., and Neel, M. C. (2013). The power to detect recent fragmentation
847 events using genetic differentiation methods. *PLoS One*, 8(5):e63981.

848 Lourenço, A., Álvarez, D., Wang, I. J., and Velo-Antón, G. (2017). Trapped within the city:
849 Integrating demography, time since isolation and population-specific traits to assess the genetic
850 effects of urbanization. *Molecular Ecology*, 26(6):1498–1514.

851 Maebe, K., Meeus, I., Vray, S., Claeys, T., Dekoninck, W., Boevé, J.-L., Rasmont, P., and Smagghe,
852 G. (2016a). A century of temporal stability of genetic diversity in wild bumblebees. *Scientific*
853 *Reports*, 6(1):38289.

854 Maebe, K., Meeus, I., Vray, S., Claeys, T., Dekoninck, W., Boevé, J.-L., Rasmont, P., and Smagghe,
855 G. (2016b). A century of temporal stability of genetic diversity in wild bumblebees. *Scientific*
856 *Reports*, 6(1):38289.

857 Maruyama, T. and Fuerst, P. A. (1985). Population bottlenecks and nonequilibrium models in
858 population genetics. ii. number of alleles in a small population that was formed by a recent
859 bottleneck. *Genetics*, 111(3):675–689.

860 Mazet, O., Rodríguez, W., Grusea, S., Boitard, S., and Chikhi, L. (2016). On the importance
861 of being structured: instantaneous coalescence rates and human evolution—lessons for ancestral
862 population size inference? *Heredity*, 116(4):362–371.

863 Miller, E. F., Green, R. E., Balmford, A., Maisano Delser, P., Beyer, R., Somveille, M., Leonardi,
864 M., Amos, W., and Manica, A. (2021). Bayesian skyline plots disagree with range size changes
865 based on species distribution models for holarctic birds. *Molecular Ecology*, 30(16):3993–4004.

866 Nadachowska-Brzyska, K., Li, C., Smeds, L., Zhang, G., and Ellegren, H. (2015). Temporal dynamics
867 of avian populations during pleistocene revealed by whole-genome sequences. *Current Biology*,
868 25(10):1375–1380.

Natesh, M., Vinay, K., Ghosh, S., Jayapal, R., Mukherjee, S., Vijay, N., and Robin, V. (2020). Contrasting trends of population size change for two eurasian owlet species—athene brama and glaucidium radiatum from south asia over the late quaternary. *Frontiers in Ecology and Evolution*, 8:608339.

Nei, M., Maruyama, T., and Chakraborty, R. (1975). The bottleneck effect and genetic variability in populations. *Evolution*, pages 1–10.

Nikolic, N. and Chevalet, C. (2014). Detecting past changes of effective population size. *Evolutionary applications*, 7(6):663–681.

Notohara, M. (1990). The coalescent and the genealogical process in geographically structured population. *Journal of mathematical biology*, 29:59–75.

Nyström, V., Angerbjörn, A., and Dalén, L. (2006). Genetic consequences of a demographic bottleneck in the scandinavian arctic fox. *Oikos*, 114(1):84–94.

Ohta, T. and Kimura, M. (1973). A model of mutation appropriate to estimate the number of electrophoretically detectable alleles in a finite population. *Genetics Research*, 22(2):201–204.

Pacifici, M., Rondinini, C., Rhodes, J. R., Burbidge, A. A., Cristiano, A., Watson, J. E., Woinarski, J. C., and Di Marco, M. (2020). Global correlates of range contractions and expansions in terrestrial mammals. *Nature Communications*, 11(1):2840.

Pacifici, M., Santini, L., Di Marco, M., Baisero, D., Francucci, L., Marasini, G. G., Visconti, P., and Rondinini, C. (2013). Generation length for mammals. *Nature Conservation*, 5:89–94.

Parreira, B. R. and Chikhi, L. (2015). On some genetic consequences of social structure, mating systems, dispersal, and sampling. *Proceedings of the National Academy of Sciences*, 112(26):E3318–E3326.

Peters, R. H. and Peters, R. H. (1986). *The ecological implications of body size*, volume 2. Cambridge university press.

Pflüger, F. J., Signer, J., and Balkenhol, N. (2019). Habitat loss causes non-linear genetic erosion in specialist species. *Global Ecology and Conservation*, 17:e00507.

Postaire, B. D., Devloo-Delva, F., Brunnschweiler, J. M., Charvet, P., Chen, X., Cliff, G., Daly, R., Drymon, J. M., Espinoza, M., Fernando, D., et al. (2023). Global genetic diversity and historical demography of the bull shark. *Journal of Biogeography*.

Rasteiro, R., Bouttier, P.-A., Sousa, V. C., and Chikhi, L. (2012). Investigating sex-biased migration during the neolithic transition in europe, using an explicit spatial simulation framework. *Proceedings of the Royal Society B: Biological Sciences*, 279(1737):2409–2416.

Ray, N., Currat, M., Foll, M., and Excoffier, L. (2010). Splatche2: a spatially explicit simulation framework for complex demography, genetic admixture and recombination. *Bioinformatics*, 26(23):2993–2994.

Rogan, J. E., Parker, M. R., Hancock, Z. B., Earl, A. D., Buchholtz, E. K., Chyn, K., Martina, J., and Fitzgerald, L. A. (2023). Genetic and demographic consequences of range contraction patterns during biological annihilation. *Scientific Reports*, 13(1):1691.

Salmona, J., Heller, R., Quéméré, E., and Chikhi, L. (2017). Climate change and human colonization triggered habitat loss and fragmentation in madagascar. *Molecular Ecology*, 26(19):5203–5222.

Santini, L., Di Marco, M., Visconti, P., Baisero, D., Boitani, L., and Rondinini, C. (2013). Ecological correlates of dispersal distance in terrestrial mammals. *Hystrix*, 24(2).

Schlötterer, C., Ritter, R., Harr, B., and Brem, G. (1998). High mutation rate of a long microsatellite allele in drosophila melanogaster provides evidence for allele-specific mutation rates. *Molecular Biology and Evolution*, 15(10):1269–1274.

Schmitt, T. (2007). Molecular biogeography of europe: Pleistocene cycles and postglacial trends. *Frontiers in zoology*, 4:1–13.

Schneider, N., Chikhi, L., Currat, M., and Radespiel, U. (2010). Signals of recent spatial expansions in the grey mouse lemur (microcebus murinus). *BMC Evolutionary Biology*, 10(1):1–17.

Sgarlata, G. M., Maié, T., de Zoeten, T., Rasteiro, R., and Chikhi, L. (2022a). The effect of habitat loss and fragmentation on isolation-by-distance and time. *bioRxiv*, pages 2022–10.

Sgarlata, G. M., Maié, T., de Zoeten, T., Rasteiro, R., and Chikhi, L. (2022b). On the genetic consequences of habitat contraction: edge effects and habitat loss. *bioRxiv*, pages 2022–10.

Silva, M. and Downing, J. A. (1995). The allometric scaling of density and body mass: a nonlinear relationship for terrestrial mammals. *The American Naturalist*, 145(5):704–727.

Smith, J. M. and Slatkin, M. (1973). The stability of predator-prey systems. *Ecology*, 54(2):384–391.

Sommer, R. S. and Nadachowski, A. (2006). Glacial refugia of mammals in europe: evidence from fossil records. *Mammal Review*, 36(4):251–265.

Srinivas, Y. and Jhala, Y. (2023). Genetic diversity, structure, and demographic histories of unique and ancient wolf lineages in india. *Conservation Genetics*, pages 1–16.

Storz, J. F. and Beaumont, M. A. (2002). Testing for genetic evidence of population expansion and contraction: an empirical analysis of microsatellite dna variation using a hierarchical bayesian model. *Evolution*, 56(1):154–166.

Sugg, D. W., Chesser, R. K., Stephen Dobson, F., and Hoogland, J. L. (1996). Population genetics meets behavioral ecology. *Trends in Ecology & Evolution*, 11(8):338–342.

Svenning, J.-C., Eiserhardt, W. L., Normand, S., Ordonez, A., and Sandel, B. (2015). The influence of paleoclimate on present-day patterns in biodiversity and ecosystems. *Annual Review of Ecology, Evolution, and Systematics*, 46:551–572.

Szép, E., Trubenová, B., and Csilléry, K. (2022). Using gridcoal to assess whether standard population genetic theory holds in the presence of spatio-temporal heterogeneity in population size. *Molecular Ecology Resources*, 22(8):2941–2955.

Taron, U. H., Salado, I., Escobar-Rodríguez, M., Westbury, M. V., Butschkau, S., Paijmans, J. L., VonHoldt, B. M., Hofreiter, M., and Leonard, J. A. (2021). A sliver of the past: The decimation of the genetic diversity of the mexican wolf. *Molecular ecology*, 30(23):6340–6354.

Team, R. C. et al. (2016). R: A language and environment for statistical computing. r foundation for statistical computing, vienna, austria. *http://www. R-project. org/*.

Teixeira, H., Montade, V., Salmona, J., Metzger, J., Bremond, L., Kasper, T., Daut, G., Rouland, S., Ranarilalatiana, S., Rakotondravony, R., et al. (2021). Past environmental changes affected lemur population dynamics prior to human impact in madagascar. *Communications biology*, 4(1):1084.

Townsend, A. K., Jones, M. L., Chen, N., Chivily, C., McAndrews, C., Clark, A. B., McGowan, K. J., and Eimes, J. (2023). Increased genetic diversity and immigration after west nile virus emergence in american crows: No evidence for a genetic bottleneck. *Molecular Ecology*.

Wakeley, J. (1999). Nonequilibrium migration in human history. *Genetics*, 153(4):1863–1871.

Walton, W., Stone, G. N., and Lohse, K. (2021). Discordant pleistocene population size histories in a guild of hymenopteran parasitoids. *Molecular Ecology*, 30(18):4538–4550.

Wang, P., Hou, R., Wu, Y., Zhang, Z., Que, P., and Chen, P. (2022). Genomic status of yellow-breasted bunting following recent rapid population decline. *Iscience*, 25(7):104501.

Welch, A. J., Wiley, A. E., James, H. F., Ostrom, P. H., Stafford Jr, T. W., and Fleischer, R. C. (2012). Ancient dna reveals genetic stability despite demographic decline: 3,000 years of population history in the endemic hawaiian petrel. *Molecular biology and evolution*, 29(12):3729–3740.

Wolf, C. and Ripple, W. J. (2017). Range contractions of the world's large carnivores. *Royal Society open science*, 4(7):170052.

Figures

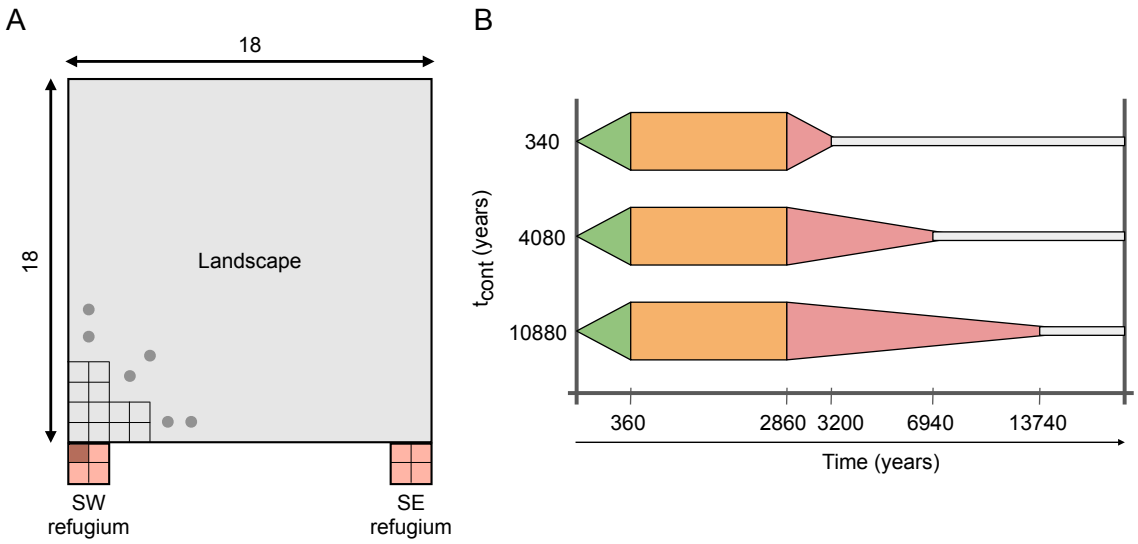

Figure 1: **Simulated landscape and habitat change scenarios:** Panel A) The simulated 2D landscape consists of 18×18 demes with two refuge areas (SW and SE refugium) of 2×2 demes. The red-grey deme (top-left deme in SW refugium) corresponds to the ancestral population from which the spatial expansion starts. Panel B) Schematic representation of habitat changes over time, assuming an initial phase of expansion (green), after which habitat remains stationary (orange) before contraction (red). We considered three different scenarios characterized by the same expansion and stationary periods but different contraction durations (t_{cont}, y-axis). After the end of the contraction, the population was allowed to survive in the refuge areas. Individuals were sampled only from the refuge areas (see text for details). Altogether, the population starts with K individuals in the SW refugium, grows to a maximum possible of $324 \times$K, and decreases to two refugium populations of 4K each.

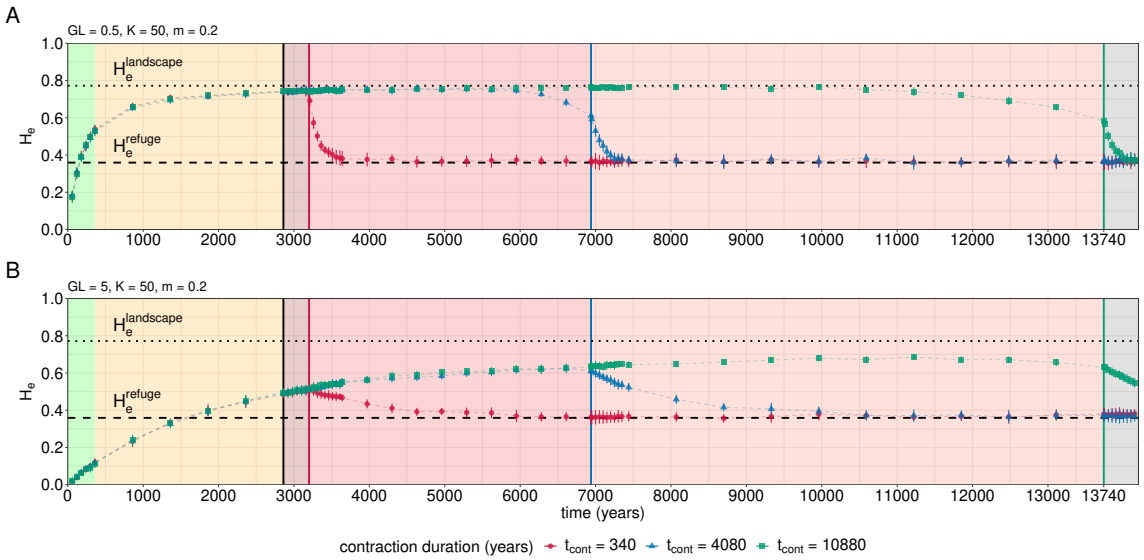

Figure 2: **Dynamics of genetic diversity in the Southwest (SW) refugium population:** Temporal evolution of H_e estimated for 40 individuals sampled in the SW refugium population at discrete times. Two generation lengths are considered: $GL = 0.5$ years (Panel A) and $GL = 5$ years (Panel B). In both panels, each point represents the average over 15 simulations, while the error bars represent the standard deviations. The discrete time points are connected by dashed lines and their symbols and colors represent the duration of the contraction phase for three scenarios, corresponding to $t_{cont} = 340$ years (red circles), $t_{cont} = 4,080$ years (blue triangles) and $t_{cont} = 10,880$ years (green squares) respectively. The dotted (resp. dashed) horizontal line represents the value of H_e at mutation-migration-drift equilibrium when the refugium (resp. entire landscape) is occupied, i.e. H_e^{refuge} ($H_e^{landscape}$). The four vertical lines, from left to right, represent the following events: i) start of the contraction phase (black, time $= 2,860$ years for all scenarios) and end of the contraction phase for (ii) $t_{cont} = 340$ years (red, time $= 3,200$ years) iii) $t_{cont} = 4,080$ years (blue, time $= 6,940$ years) and iv) $t_{cont} = 10,880$ years (green, time $= 13,740$ years). The other parameter values for both plots are (K, m)=$(50, 0.2)$. Panel B shows that when contraction is slow (here $10,880$ years), H_e can keep increasing for more than $7,000$ years after contraction started and keep high and stable levels of genetic diversity that are much higher than H_e^{refuge} for more than $10,000$ years.

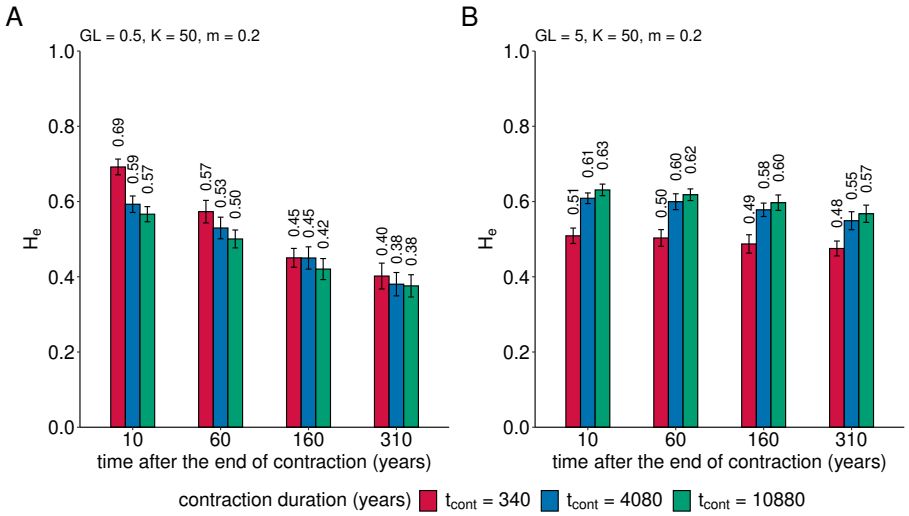

Figure 3: H_e **in the SW refugium population at the end of contraction:** Two generation lengths are considered: $GL = 0.5$ years (Panel A) and $GL = 5$ years (Panel B). In both panels, colors represent the duration of the contraction phase for three scenarios, corresponding to $t_{cont} = 340$ years (red), $t_{cont} = 4,080$ years (blue), and $t_{cont} = 10,880$ years (green) respectively. The height of the histogram bars represents the means and the error bars represent the standard deviations measured across 15 simulations. The other parameter values for both plots are (K, m)=$(50, 0.2)$. Panel A suggests that quick contraction "maintains" more genetic diversity than slow contraction. Panel B suggests the opposite with a significant difference even when populations are sampled 310 years after the end of contraction.

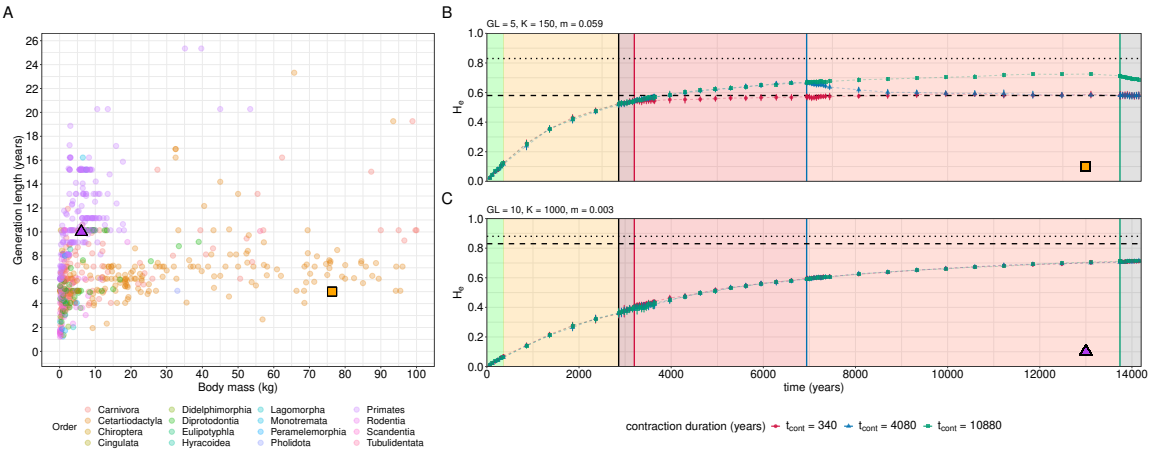

Figure 4: **Life-history traits and dynamics of H_e in SW refugium:** Panel A: Generation length as a function of body mass across different orders of mammalian species (data from (Pacifici et al., 2013)). Panels B-C: Temporal dynamics of H_e in the SW refugium population for 40 individuals sampled at discrete times. Panel B represents a species with ($GL = 5$ years, $K = 150$ and $m = 0.059$, orange square in panel A) whereas Panel C represents a species with ($GL = 10$ years, $K = 1,000$ and $m = 0.003$, violet triangle in panel A). Colors, symbols, and lines in panels B and C encode the same information as in Figure 2.

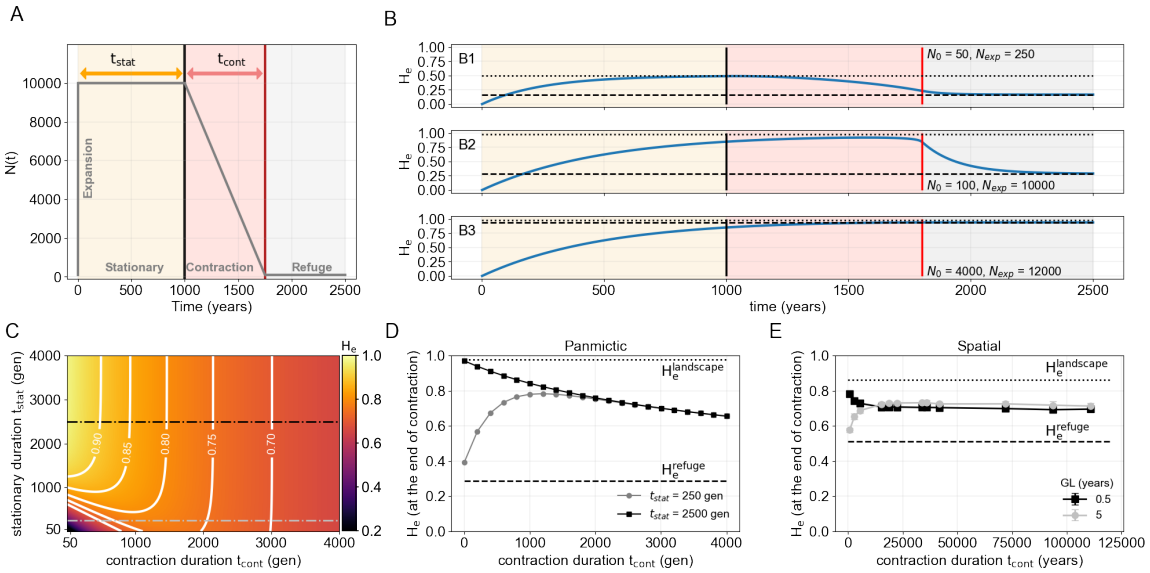

Figure 5: **Genetic diversity in the panmictic model and spatial simulation validation:** Panel A: Schematic representation of population size changes in our panmictic single population model. Panel B: Time evolution of H_e in a panmictic population under size changes represented in panel A. Three distinct temporal dynamics of H_e are observed by changing the initial (N_0) and expanded population (N_{exp}) sizes, keeping other parameters constant. The N_0 represents the refugium population size and N_{exp} represents the population size when the whole habitat is colonized. Specifically, we set $(N_0, N_{exp}) = (50, 250)$ (Panel B1), $(N_0, N_{exp}) = (100, 10000)$ (Panel B2) and $(N_0, N_{exp}) = (4000, 12000)$ (Panel B3), three scenarios corresponding to a five, hundred and three-fold increase in population size, respectively. In the three subpanels (B1, B2, and B3), the two vertical lines, from left to right, represent the following events, respectively: i) the start of the contraction phase (black, time $= 1,000$ years) and ii) the end of contraction (red, time $= 1,800$ years). Panel C: H_e estimated at the end of the contraction phase, as a function of the duration of the contraction (x-axis, t_{cont}) and stationary (y-axis, t_{stat}) phases. The two horizontal dot-dashed lines represent two transects for two t_{stat} values, $t_{stat} = 2,500$ generations (black) and $t_{stat} = 250$ generations (grey). Panel D: H_e estimated at the end of contraction as a function of contraction durations, for two stationary times, $t_{stat} = 2,500$ generations (black squares) and $t_{stat} = 250$ generations (grey circles), represented by the dashed horizontal lines in Panel C. Panels C and D were obtained for $(N_0, N_{exp}) = (100, 10000)$, *i.e.* a scenario with two orders of magnitude change in population size. Panel E: Spatial simulation analysis: H_e estimated at the end of contraction for ($t_{stat} = 2,500$ years) as a function of contraction duration. The lines and symbols correspond to two generation lengths, $GL = 0.5$ years (black, $5,000$ generations in stationary phase) and $GL = 5$ years (grey, 500 generations in stationary phase). Each point represents the mean and the error bars represent the standard deviations measured across 15 simulations. The other parameters for the spatial simulations are set to (K, m)=$(100, 0.2)$.